



TEXAS
The University of Texas at Austin

Austin COVID-19 transmission estimates and healthcare projections

Mauricio Tec*, Michael Lachmann*, Spencer J. Fox*, Remy Pasco, Spencer Woody, Jennifer Starling, Maytal Dahan, Kelly Gaither, James Scott, Lauren Ancel Meyers

The University of Texas at Austin
COVID-19 Modeling Consortium
utpandemics@austin.utexas.edu

Austin COVID-19 transmission estimates and healthcare projections

[The University of Texas COVID-19 Modeling Consortium](#)

Contributors: Mauricio Tec*, Michael Lachmann*, Spencer J. Fox*, Remy Pasco, Spencer Woody, Jennifer Starling, Maytal Dahan, Kelly Gaither, James Scott, Lauren Ancel Meyers

* Authors contributed equally

Contact: utpandemics@austin.utexas.edu

Overview

To support public health decision-making and healthcare planning, we developed a model for the five-county Austin-Round Rock Metropolitan Statistical Area (henceforth *Austin*) that can provide real-time estimates of the prevalence and transmission rate of COVID-19 and project healthcare needs into the future.

The model incorporates key epidemiological characteristics of the disease, demographic information for Austin, and local mobility data from anonymized cell phone traces. It uses daily COVID-19 hospitalization data to estimate the changing transmission rate and prevalence of disease. The framework can be readily applied to provide pandemic situational awareness and short-term healthcare projections in other cities around the US.

In this report, we use COVID-19 hospitalization data for Austin from March 13 to July 14, 2020 to estimate the state of the pandemic in early July and project hospitalizations through early August of 2020. The projections are based on multiple assumptions about the age-specific severity of COVID-19 and the role of asymptomatic infections in the transmission of the virus. These graphs below do not present the full range of uncertainty for the city of Austin, but are intended to provide basic insight into the changing risks of COVID-19 transmission and healthcare surges in Austin.

Our estimates suggest that the pandemic slowed considerably during the March 24-May 1, 2020 stay-home order and reached its lowest transmission rate in mid April. As Texas began relaxing social distancing measures in early May, transmission picked up and continued to increase through mid June. The recent decrease in transmission may have stemmed from mid-June tightening of restrictions and an increase in cautionary

messaging. Our projections suggest that, if the pandemic continues to spread at the rate estimated from the second week of July, COVID-19 hospitalizations and/or ICU demands could exceed local capacity in early August.

We are posting these results prior to peer review to provide intuition for both policy makers and the public regarding both the immediate threat of COVID-19 and the extent to which continued social distancing, transmission-reducing precautions such as keeping physical distance, wearing cloth face coverings and staying isolated when symptomatic, can mitigate that threat.

As new hospitalization data become available, we will provide updated estimates and projections on the UT COVID-19 Modeling Consortium's [Austin COVID-19 Dashboard](#).

Austin COVID-19 model

The appendix below describes the model in detail. In short, we use mathematical equations to track the changing numbers of individuals who are susceptible (not yet infected), infected, hospitalized, recovered, and deceased. The model incorporates key features of the virus and uses iterated filtering [1] to estimate daily transmission rates in Austin from a combination of local hospital data (COVID-19 admissions, discharges and deaths) as well as SafeGraph mobility trends (cell phone-based estimates of hours spent at home and daily trips to public points-of-interest such as grocery stores, restaurants, bars and parks [2]). We use the estimated transmission rates to project COVID-19 cases, hospitalizations, ICU visits and deaths several weeks ahead. The model makes the following assumptions:

- Epidemic seeding: February 17th, 2020 with 1 infected adult
- Transmission rates are modulated by age-specific contact patterns
- Following infection, cases go through multiple stages of infection:

Stage 1: Pre-symptomatic and non-contagious for an average of 2.9 days

Stage 2: Pre-symptomatic contagious for an average of 2.3 days (44% of transmission events occur during this period)

Stage 3: Symptomatic contagious or asymptomatic contagious for an average of 4 days. The model assumes that 43% of all infections are asymptomatic and that asymptomatic cases are 67% as infectious as symptomatic cases.

- Cases may be hospitalized and/or die at rates that depend on their age and risk group.
 - The overall infection hospitalization rate (IHR) is 4.2%
 - The overall infection fatality rate (IFR) is 0.54%
- The duration of hospital stays are estimated from the local hospitalization data and can change through time.

The pace of COVID-19 spread in Austin to July 14, 2020

We track COVID-19 spread in Austin through a metric called the effective reproduction number, $R(t)$. This indicates the contagiousness of the virus at a given point time and roughly corresponds to the average number of people a typical case will infect.

Measures to slow or prevent transmission, such as social distancing and mask wearing, can reduce the reproduction number. Immunity acquired either through past infection or vaccination can also reduce the reproduction number. If $R(t)$ is greater than one, then an epidemic will continue to grow; if $R(t)$ is less than one, it will begin to subside. By tracking $R(t)$, we can detect whether policies and individual-level behaviors are having the desired impact and project cases, hospitalizations and deaths into the future.

We estimate that the initial reproduction number of COVID-19 in early March (prior to social distancing measures) was 5.3 [95% CrI: 4.1-6.6]. Following the March 24th stay-home order, it rapidly declined to a minimum value of 0.8 [95% CrI: 0.6-1.1] during the week of April 17-24 (Figure 1 and Table 1). From May 1st to mid-June, the reproduction number increased, fueling a surge in cases and hospitalizations, reaching 1.6 [95% CrI: 1.4-1.8] the week of June 12-19. It has since declined, dropping to 0.8 [95% CrI: 0.4-1.8] as of July 7-14, 2020.

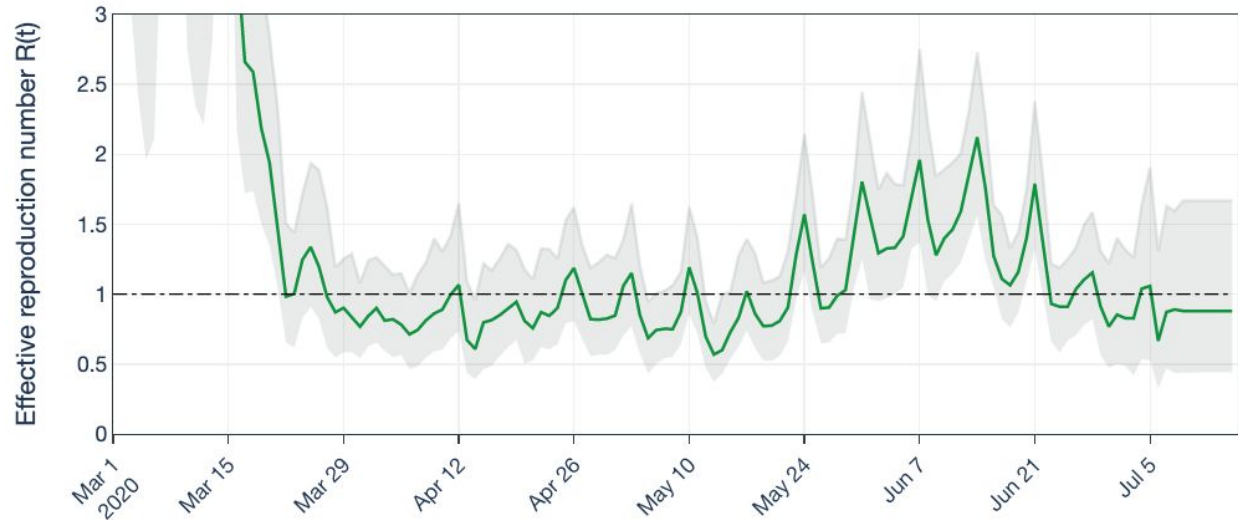


Figure 1: The estimated effective reproduction number, $R(t)$, of the COVID-19 pandemic in Austin from February 17, 2020 to July 14, 2020. $R(t)$ is an epidemiological quantity used to describe the contagiousness of a disease. An epidemic is expected to continue if $R(t)$ is greater than one and to end if $R(t)$ is less than one. This *epidemic threshold* of $R(t) = 1$ is indicated by a horizontal dashed line. $R(t)$ can be interpreted as the average number of people that an infected case will infect. The value of $R(t)$ depends on the basic infectiousness of the disease, the number of people that are susceptible to infection, and the impact of social distancing, mask wearing and other measures to slow transmission. The solid line gives the mean daily estimate and the shaded ribbon indicates the 95% credible interval. The apparent weekly cyclicity is caused by weekday-weekend fluctuations in mobility.

Table 1: Estimated effective reproduction number $R(t)$ at the beginning of the pandemic, prior to the March 24th stay-home order (highest value), during the midst of the stay-home order (lowest value), during the early-June pandemic rebound, and the week of July 7-14, 2020.

	Week ending on	$R(t)$ (95% CrI)
Highest value estimated	March 13, 2020	5.3 (4.1 - 6.6)
Lowest value estimated	April 24, 2020	0.8 (0.6 - 1.1)
Mid-June peak	June 19, 2020	1.6 (1.4 - 1.8)
Current	July 14, 2020	0.8 (0.4 - 1.8)

COVID-19 healthcare projections for Austin

Based on the transmission rates estimated for the second week of July, we project the numbers of COVID-19 hospitalizations and ICU patients through early August (Figures 2-4). We estimate that the reproduction number is slightly below one but could be a bit above one (Table 1 and Figure 1). Our *spaghetti line* projections in each figure capture this uncertainty. Some trend upwards while others trend downwards. Each line represents an equally likely future path. The bold line in each graph indicates the median across the different trends.

The Austin Executive COVID-19 Task Force has estimated that across all hospitals in the five-county metropolitan area, the maximum COVID-19 hospital surge capacity is 1,500 patients and the maximum COVID-19 ICU surge capacity is somewhere between 331 and 474 patients. Recent COVID-19 hospitalization data suggest that between 30% and 40% of hospitalized COVID-19 patients are in ICU's. The model projections for August 1st (assuming policies and behavior do not change) are that daily hospital admissions will reach 58 [95% CrI: 14-234], total daily COVID-19 hospitalizations will reach 446 [95% CrI: 172-1,445], and total daily COVID-19 ICU patients will reach 156 [95% CrI: 60-506].



Figure 2: Projected seven-day rolling average in COVID-19 hospital admissions in the Austin-Round Rock MSA through August 11, 2020. Green points represent the reported daily values for all Austin area hospitals; green lines represent the rolling seven-day average. Grey “spaghetti” lines represent equally likely projections and the bold blue line indicates the median trend, based on the range of transmission rates estimated for July 7-14, 2020 (Table 1). Differences between lines are caused by uncertainty in the model inputs as well as variation in individual behavior and disease progression.



Figure 3: Projected COVID-19 hospitalizations in the Austin-Round Rock MSA through August 11, 2020. Green points represent the reported daily census. Grey “spaghetti” lines represent equally likely projections and the blue line indicates the median trend based on the range of transmission rates estimated for July 7-14, 2020 (Table 1). Differences between lines are caused by uncertainty in the model inputs as well as variation in individual behavior and disease progression.



Figure 4: Projected COVID-19 ICU patients in the Austin-Round Rock MSA through August 11, 2020. Green points represent the reported daily census. Grey “spaghetti” lines represent equally likely projections and the blue line indicates the median trend based on the range of transmission rates estimated for July 7-14, 2020 (Table 1). These projections assume that 35% of hospitalized COVID-19 patients are in the ICU. Differences between lines are caused by uncertainty in the model inputs as well as variation in individual behavior and disease progression.

Appendix

COVID-19 Epidemic Model Structure and Parameters

The model structure is diagrammed in Figure A1 and described in the equations below. For each age and risk group, we build a separate set of compartments to model the transitions between the states: susceptible (S), exposed (E), pre-symptomatic infectious (P^Y), pre-asymptomatic infectious (P^A), symptomatic infectious (I^Y), asymptomatic infectious (I^A), symptomatic infectious that are hospitalized (I^H), recovered (R), and deceased (D). The symbols S, E, P^Y , P^A , I^Y , I^A , I^H , R, and D denote the number of people in that state in the given age/risk group and the total size of the age/risk group is

$$N = S + E + P^Y + P^A + I^Y + I^A + I^H + R + D.$$

The deterministic model for individuals in age group a and risk group r is given by:

$$\begin{aligned} \frac{dS_{a,r}}{dt} &= -S_{a,r} \cdot \sum_{i \in A} \sum_{j \in K} (I_{i,j}^Y \omega^Y + I_{i,j}^A \omega^A + P_{i,j}^Y \omega^{PY} + P_{i,j}^A \omega^{PA}) \beta(t) \phi_{a,i} / N_i \\ \frac{dE_{a,r}}{dt} &= S_{a,r} \cdot \sum_{i \in A} \sum_{j \in K} (I_{i,j}^Y \omega^Y + I_{i,j}^A \omega^A + P_{i,j}^Y \omega^{PY} + P_{i,j}^A \omega^{PA}) \beta(t) \phi_{a,i} / N_i - \sigma E_{a,r} \\ \frac{dP_{a,r}^A}{dt} &= (1 - \tau) \sigma E_{a,r} - \rho^A P_{a,r}^A \\ \frac{dP_{a,r}^Y}{dt} &= \tau \sigma E_{a,r} - \rho^Y P_{a,r}^Y \\ \frac{dI_{a,r}^A}{dt} &= \rho^A P_{a,r}^A - \gamma^A I_{a,r}^A \\ \frac{dI_{a,r}^Y}{dt} &= \rho^Y P_{a,r}^Y - (1 - \pi) \gamma^Y I_{a,r}^Y - \pi \eta I_{a,r}^Y \\ \frac{dI_{a,r}^H}{dt} &= \pi \eta I_{a,r}^Y - (1 - \nu) \gamma^H(t) I_{a,r}^H - \nu \mu(t) I_{a,r}^H \\ \frac{dR_{a,r}}{dt} &= \gamma^A I_{a,r}^A + (1 - \pi) \gamma^Y I_{a,r}^Y + (1 - \nu) \gamma^H(t) I_{a,r}^H \\ \frac{dD_{a,r}}{dt} &= \nu \mu(t) I_{a,r}^H \end{aligned}$$

where A and K are all possible age and risk groups, ω^A , ω^Y , ω^{PA} , ω^{PY} are the relative infectiousness of the I^A , I^Y , I^{PA} , I^{PY} compartments, respectively, β is transmission rate, $\phi_{a,i}$ is the mixing rate between age group a , $i \in A$, and γ^A , γ^Y , $\gamma^H(t)$ are the recovery rates for the

I^A , I^Y , I^H compartments, respectively, σ is the exposed rate, ρ^A, ρ^Y are the pre-(a)symptomatic rates, τ is the symptomatic ratio, π is the proportion of symptomatic individuals requiring hospitalization, η is rate at which hospitalized cases enter the hospital following symptom onset, ν is mortality rate for hospitalized cases, and $\mu(t)$ is daily instantaneous rate at which terminal patients die.

We simulate the model using a stochastic implementation of the deterministic equations. Transitions between compartments are governed using the τ -leap method [3,4] with key parameters given in Table A1-2. We simulate the model according to the following equations:

$$\begin{aligned} S_{a,r}(t+1) - S_{a,r}(t) &= -P_1 \\ E_{a,r}(t+1) - E_{a,r}(t) &= P_1 - P_2 \\ P_{a,r}^A(t+1) - P_{a,r}^A(t) &= (1 - \tau)P_2 - P_3 \\ P_{a,r}^Y(t+1) - P_{a,r}^Y(t) &= \tau P_2 - P_4 \\ I_{a,r}^A(t+1) - I_{a,r}^A(t) &= P_3 - P_5 \\ I_{a,r}^Y(t+1) - I_{a,r}^Y(t) &= P_4 - P_6 - P_7 \\ I_{a,r}^H(t+1) - I_{a,r}^H(t) &= P_7 - P_8 - P_9 \\ R_{a,r}(t+1) - R_{a,r}(t) &= P_5 + P_6 + P_8 \end{aligned}$$

with

$$\begin{aligned} P_1 &\sim B(n = S_{a,r}(t), p = 1 - e^{-(F_{a,r}(t)) \cdot dt}) \\ P_2 &\sim B(n = E_{a,r}(t), p = 1 - e^{-(\sigma) \cdot dt}) \\ P_3 &\sim B(n = P_{a,r}^A(t), p = 1 - e^{-(\rho^A) \cdot dt}) \\ P_4 &\sim B(n = P_{a,r}^Y(t), p = 1 - e^{-(\rho^Y) \cdot dt}) \\ P_5 &\sim B(n = I_{a,r}^A(t), p = 1 - e^{-(\gamma^A) \cdot dt}) \\ P_6 &\sim B(n = I_{a,r}^Y(t), p = 1 - e^{-((1-\pi)\gamma^Y) \cdot dt}) \\ P_7 &\sim B(n = I_{a,r}^Y(t), p = 1 - e^{-(\pi\eta) \cdot dt}) \\ P_8 &\sim B(n = I_{a,r}^H, p = 1 - e^{-((1-\nu)\gamma^H(t)) \cdot dt}) \\ P_9 &\sim B(n = I_{a,r}^H(t), p = 1 - e^{-(\nu\mu(t)) \cdot dt}) \end{aligned}$$

where $B(n,p)$ denotes a binomial distribution with n trials each with probability of success p . $F_{a,r}^I$ denotes the force of infection for individuals in age group a and risk group r and is given by

$$F_{a,r}(t) = \sum_{i \in A} \sum_{j \in K} (I_{i,r}^Y(t)\omega^Y + I_{i,r}^A(t)\omega^A + P_{i,j}^Y(t)\omega^{PY} + P_{i,j}^A(t)\omega^{PA})\beta(t)\phi_{a,i}/N_i$$

with

$$\beta(t) = e^{\log(\beta(0)) + b_1(t) \cdot PC1 + b_2(t) \cdot PC2 + Z(t)}$$

$$b_1(t) \sim N(b_1(t-1), \sigma_{b_1})$$

$$b_2(t) \sim N(b_2(t-1), \sigma_{b_2})$$

$$Z(t) \sim N(0.97 \cdot Z(t-1), \sigma_Z), Z(0) = 0.$$

where PC1 and PC2 describe the first and second principal components from our mobility data as described below. Finally,

$$\mu(t) = e^{\log(\mu(0)) + Z_\mu} \text{ where } Z_\mu(t) \sim N(\psi_\mu \cdot Z_\mu(t-1), \sigma_\mu), Z_\mu(0) = 0 \text{ and}$$

$$\gamma^H(t) = e^{\log(\gamma^H(0)) + Z_\gamma} \text{ where } Z_\gamma(t) \sim N(0.99 \cdot Z_\gamma(t-1), \sigma_\gamma), Z_\gamma(0) = 0.$$

We estimate $\beta(t)$, k , σ_Z , $b_1(t)$, $b_2(t)$, σ_{b_1} , σ_{b_2} , ψ_μ , σ_μ , and σ_γ as described in the model fitting section below.

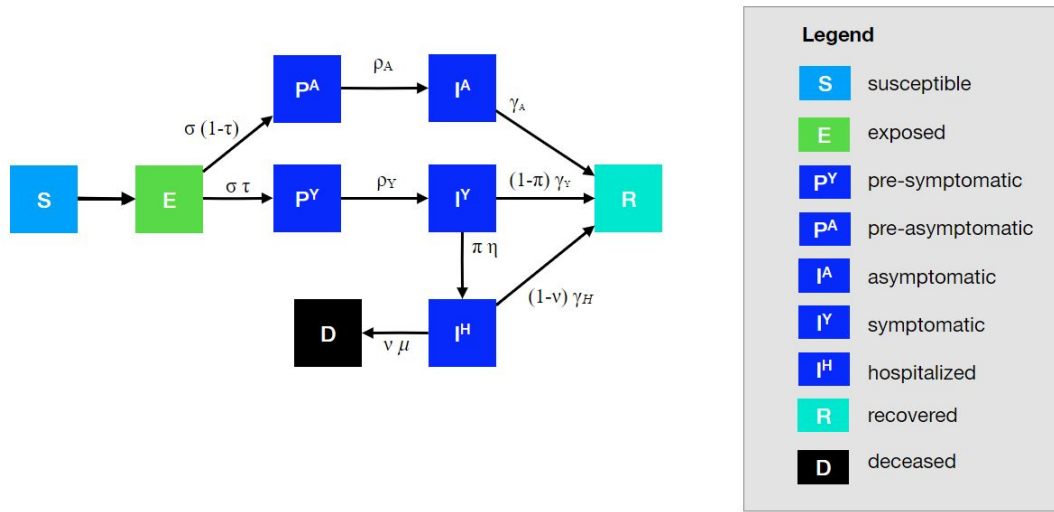


Figure A1. Compartmental model of COVID-19 transmission in the Austin MSA. Each subgroup (defined by age and risk) is modeled with a separate set of compartments. Upon infection, susceptible individuals (S) progress to exposed (E) and then to either pre-symptomatic infectious (P^Y) or pre-asymptomatic infectious (P^A) from which they move to symptomatic infectious (I^Y) and asymptomatic infectious (I^A) respectively. All asymptomatic cases eventually progress to a recovered class where they remain protected from future infection (R); symptomatic cases are either hospitalized (I^H) or recover. Mortality (D) varies by age group and risk group and is assumed to be preceded by hospitalization.

Mobility trends

We used mobility trends data from the Austin MSA to inform the transmission rate in our model. Specifically, we ran a principal component analysis (PCA) on eight independent mobility variables provided by SafeGraph, including home dwell time and visits to universities, bars, grocery stores, museums and parks, medical facilities, schools, and restaurants [2]. We regressed the transmission rate on the first two principal components from the mobility data as described in the modeling equations for $\beta(t)$.

Epidemic starting conditions

We could not estimate the epidemic start date directly using our model, because the transmission rate flexibility gave rise to similarly good fits within a wide-range of potential values for t_0 . We therefore conducted an independent estimation procedure to obtain reasonable epidemic start dates for Austin. We then used our best guess parameters as described in Table A2 and chose $\beta(0) = 0.67$ as it produced three-day doubling rate in cumulative cases and gave $R_t(0) = 4$ which are consistent with observations for the Austin early outbreak dynamics [5]. We ran 1,000 stochastic simulations with these initial conditions, and identified the wait time for when there was 1 admit for Austin. We estimated the start time from the resulting distribution of wait times for Austin as February 17, 2020 (IQR = February 11 - February 23), and chose February 17th, 2020 as the start date for the model.

Model likelihood

We obtained daily hospital admit ($H_A(t)$), discharge data ($H_L(t)$), total hospitalizations ($H(t)$), and death data ($H_D(t)$) for the Austin MSA. In this model we estimated $\beta(t)$, k , σ_Z , $b_1(t)$, $b_2(t)$, σ_{b_1} , σ_{b_2} , ψ_μ , σ_μ , σ_γ and fixed the remaining parameters as described in Table A1-2. We assumed all sources of data were negative binomially distributed around their predicted values from the SEIR stochastic model, and chose informative, but relatively dispersed priors for certain parameters for stability in parameter estimation and to prevent the model from overfitting data through large perturbations to time-dependent variables.

Following all of these considerations, the likelihood for our stochastic model was:

$$p(Y(t), b_1(0), \sigma_{b_1}, b_2(0), \sigma_{b_2}, k | \theta) = p(Y(t) | \theta, b_1(0), \sigma_{b_1}, b_2(0), \sigma_{b_2}, k) \cdot p(\theta, b_1(0), \sigma_{b_1}, b_2(0), \sigma_{b_2}, k)$$

where $Y(t)$ refers to the four types of data from hospitals, θ contains all parameters from Table A1 not explicitly listed, and where

$$p(Y(t) | \theta, b_1(0), \sigma_{b_1}, b_2(0), \sigma_{b_2}, k) = p(H_A(t) | \hat{H}_A(t)) p(H_L(t) | \hat{H}_L(t)) p(H_D(t) | \hat{H}_D(t)) p(H(t) | \hat{H}(t))$$

$$p(\theta, b_1(0), \sigma_{b_1}, b_2(0), \sigma_{b_2}, k) = p(b_1(0)) \cdot p(\sigma_{b_1}) \cdot p(b_2(0)) \cdot p(\sigma_{b_2}) \cdot p(k)$$

with

$$p(H_A(t) | \hat{H}_A(t)) = \binom{k + H_A(t) - 1}{H_A(t)} \cdot p^k (1 - p)^{H_A(t)}, \text{ and } p = \frac{k}{k + \hat{H}_A(t)}$$

$$p(H_L(t) | \hat{H}_L(t)) = \binom{k + H_L(t) - 1}{H_L(t)} \cdot p^k (1 - p)^{H_L(t)}, \text{ and } p = \frac{k}{k + \hat{H}_L(t)}$$

$$p(H_D(t) | \hat{H}_D(t)) = \binom{k + H_D(t) - 1}{H_D(t)} \cdot p^k (1 - p)^{H_D(t)}, \text{ and } p = \frac{k}{k + \hat{H}_D(t)}$$

$$p(H(t)|\hat{H}(t)) = \binom{k + H(t) - 1}{H(t)} \cdot p^k (1 - p)^{H(t)}, \text{ and } p = \frac{k}{k + \hat{H}(t)}$$

$$p(b_1(0)) \cdot t_d = \frac{1}{\sqrt{2}} e^{-\frac{1}{2}(\hat{b}_1(0))^2}$$

$$p(b_2(0)) \cdot t_d = \frac{1}{\sqrt{2}} e^{-\frac{1}{2}(\hat{b}_2(0))^2}$$

$$p(\sigma_{b_1}) \cdot t_d = \frac{1}{\Gamma(1.1) \cdot \frac{1}{1.1}} \hat{\sigma}_{b_1}^{1.1-1} e^{-1.1 \cdot \hat{\sigma}_{b_1}}$$

$$p(\sigma_{b_2}) \cdot t_d = \frac{1}{\Gamma(1.1) \cdot \frac{1}{1.1}} \hat{\sigma}_{b_2}^{1.1-1} e^{-1.1 \cdot \hat{\sigma}_{b_2}}$$

$$p(k) \cdot t_d = e^{\hat{k}}$$

and t_d is the number of days in the fitting time period.

Fitting method

In this model we estimated $\beta(t)$, k , σ_Z , $b_1(t)$, $b_2(t)$, σ_{b_1} , σ_{b_2} , ψ_μ , σ_μ , σ_γ and fixed the remaining parameters as described in Table A1. Fitting was carried out using the iterated filtering algorithm made available through the `mif2` function in the `pomp` package in R [6,7]. This algorithm is a stochastic optimization procedure; it performs maximum likelihood estimation using a particle filter to provide a noisy estimate of the likelihood for a given combination of the parameters. For each parameter combination we ran 1,000 iterations of iterated filtering, each with 10,000 particles. We calculated smoothed posterior estimates for all of the states within the model through time (including $\beta(t)$ and other time-dependent parameters which are technically state variables in our model formulation, as it changes through time according to a stochastic process). We calculated these smoothed posteriors as follows:

1. We ran 1,000 independent particle filters at the MLE, each with 10,000 particles. For each run, l , of particle filtering, we kept track of the complete trajectory of each particle, as well as the filtered estimate of the likelihood, L_l .
2. For each of the 1,000 particle filtering runs, we randomly sampled a single complete particle trajectory, giving us 1,000 separate trajectories for all state variables.
3. We resampled from these trajectories with probabilities proportional to L_l to give a distribution of state trajectories

The result can be thought of as an empirical-Bayes posterior distribution: that is, a set of 1,000 smoothed posterior draws from all state variables, conditional on the maximum likelihood estimates for the model's free parameters. This smoothed posterior distribution is how we calculate means and credible intervals for $\beta(t)$ in addition to all other time-varying state variables.

Table A1. Model parameters^a

Parameters	Value	Source
Start date	February 17, 2020	Estimated
Initial infections	1 symptomatic case age 18-49y	Assumption
$\beta(t)$: daily transmission rate	N/A	Estimated
γ^A : recovery rate on asymptomatic compartment	Equal to γ^Y	Assumption
γ^Y : recovery rate on symptomatic non-treated compartment	0.25	He et al. [8]
τ : symptomatic proportion (%)	57	Fox et al. [9]
σ : exposed rate	1/2.9	Zhang et al. [10]; He et al. [8]
ρ^A : pre-asymptomatic rate	Equal to ρ^Y	
ρ^Y : pre-symptomatic rate	$\frac{1}{2.3}$	He et al. [8]
P : proportion of pre-symptomatic transmission	44%	He et al. [8]
ω^P : relative infectiousness of pre-symptomatic individuals	$\omega^P = \frac{P}{1-P} \frac{\tau \omega^Y [Y HR / \eta + (1-Y HR) / \gamma^Y] + (1-\tau) \omega^A / \rho^A}{\tau \omega^Y / \rho^Y + (1-\tau) \omega^A / \rho^A}$ $\omega^{PY} = \omega^P \omega^Y, \omega^{PA} = \omega^P \omega^A$	
ω^A : relative infectiousness of infectious individuals in compartment I^A	$\frac{2}{3}$	He et al. [11]
IFR : infected fatality ratio, age specific (%)	Low risk: [0.0009, 0.0022, 0.0339, 0.2520, 0.6440] High risk: [0.0092, 0.0218, 0.3388, 2.5197, 6.4402]	Age adjusted from Verity et al. [12]
YFR : symptomatic fatality ratio, age specific (%)	Low risk: [0.001608, 0.003823, 0.05943, 0.4420, 1.130] High risk: [0.01608, 0.03823, 0.5943, 4.420, 11.30]	$YFR = \frac{IFR}{\tau}$

h : high-risk proportion, age specific (%)	[8.2825, 14.1121, 16.5298, 32.9912, 47.0568]	Estimated using 2015-2016 Behavioral Risk Factor Surveillance System (BRFSS) data with multilevel regression and poststratification using CDC's list of conditions that may increase the risk of serious complications from influenza [13–15]
--	--	---

^aValues given as five-element vectors are age-stratified with values corresponding to 0-4, 5-17, 18-49, 50-64, 65+ year age groups, respectively.

Table A2 Hospitalization parameters

Parameters	Value	Source
$\gamma^H(t)$: recovery rate in hospitalized compartment	Fitted	
YHR : symptomatic case hospitalization rate (%)	Low risk: [0.04021, 0.03091, 1.903, 4.114, 4.879] High risk: [0.4021, 0.3091, 19.03, 41.14, 48.79]	Age adjusted from Verity et al. [12]
π : rate of symptomatic individuals go to hospital, age-specific	$\pi = \frac{\gamma^Y * YHR}{\eta + (\gamma^Y - \eta)YHR}$	
η : rate from symptom onset to hospitalized	0.1695	5.9 day average from symptom onset to hospital admission Tindale et al. [16]
$\mu(t)$: rate from hospitalized to death	Fitted	
HFR : hospitalized fatality ratio, age specific (%)	[4, 12.365, 3.122, 10.745, 23.158]	$HFR = \frac{IFR}{\tau}$
ν : death rate on hospitalized individuals, age specific	$\nu = \frac{\gamma^H HFR}{\mu + (\gamma^H - \mu)HFR}$	
ICU : proportion hospitalized people in ICU	0.35	Estimated from Austin COVID-19 hospitalization data

Table A3 Contact matrix. Daily number contacts by age group on an average day.

	0-4y	5-17y	18-49y	50-64y	65y+
0-4y	1.88	2.02	4.01	0.79	0.28
5-17y	0.55	7.06	5.02	0.70	0.22
18-49y	0.37	2.19	8.72	1.45	0.21
50-64y	0.33	1.62	5.79	2.79	0.50
65y+	0.19	0.88	2.36	1.19	1.22

Estimation of age-stratified proportion of population at high-risk for COVID-10 complications

We estimate age-specific proportions of the population at high risk of complications from COVID-19 based on data for Austin, TX and Round-Rock, TX from the CDC's 500 cities project (Figure A2) [17]. We assume that high risk conditions for COVID-19 are the same as those specified for influenza by the CDC [13]. The CDC's 500 cities project provides city-specific estimates of prevalence for several of these conditions among adults [18]. The estimates were obtained from the 2015-2016 Behavioral Risk Factor Surveillance System (BRFSS) data using a small-area estimation methodology called multi-level regression and poststratification [14,15]. It links geocoded health surveys to high spatial resolution population demographic and socioeconomic data [15].

Estimating high-risk proportions for adults. To estimate the proportion of adults at high risk for complications, we use the CDC's 500 cities data, as well as data on the prevalence of HIV/AIDS, obesity and pregnancy among adults (Table A6).

The CDC 500 cities dataset includes the prevalence of each condition on its own, rather than the prevalence of multiple conditions (e.g., dyads or triads). Thus, we use separate co-morbidity estimates to determine overlap. Reference about chronic conditions [19] gives US estimates for the proportion of the adult population with 0, 1 or 2+ chronic conditions, per age group. Using this and the 500 cities data we can estimate the proportion of the population p_{HR} in each age group in each city with at least one chronic condition listed in the CDC 500 cities data (Table A6) putting them at high-risk for flu complications.

HIV: We use the data from table 20a in CDC HIV surveillance report [20] to estimate the population in each risk group living with HIV in the US (last column, 2015 data). Assuming independence between HIV and other chronic conditions, we increase the proportion of the population at high-risk for influenza to account for individuals with HIV but no other underlying conditions.

Morbid obesity: A BMI over 40kg/m² indicates morbid obesity, and is considered high risk for influenza. The 500 Cities Project reports the prevalence of obese people in each city with BMI over 30kg/m² (not necessarily morbid obesity). We use the data from table 1 in Sturm and Hattori [21] to estimate the proportion of people with BMI>30 that actually have BMI>40 (across the US); we then apply this to the 500 Cities obesity data to estimate the proportion of people who are morbidly obese in each city. Table 1 of Morgan et al. [22] suggests that 51.2% of morbidly obese adults have at least one other high risk chronic condition, and update our high-risk population estimates accordingly to account for overlap.

Pregnancy: We separately estimate the number of pregnant women in each age group and each city, following the methodology in CDC reproductive health report [23]. We assume independence between any of the high-risk factors and pregnancy, and further assume that half the population are women.

Estimating high-risk proportions for children. Since the 500 Cities Project only reports data for adults 18 years and older, we take a different approach to estimating the proportion of children at high risk for severe influenza. The two most prevalent risk factors for children are asthma and obesity; we also account for childhood diabetes, HIV and cancer. From Miller et al. [24], we obtain national estimates of chronic conditions in children. For asthma, we assume that variation among cities will be similar for children and adults. Thus, we use the relative prevalences of asthma in adults to scale our estimates for children in each city. The prevalence of HIV and cancer in children are taken from CDC HIV surveillance report [20] and cancer research report [25], respectively.

We first estimate the proportion of children having either asthma, diabetes, cancer or HIV (assuming no overlap in these conditions). We estimate city-level morbid obesity in children using the estimated morbid obesity in adults multiplied by a national constant ratio for each age group estimated from Hales et al. [26], this ratio represents the prevalence in morbid obesity in children given the one observed in adults. From Morgan et al. [22], we estimate that 25% of morbidly obese children have another high-risk condition and adjust our final estimates accordingly.

Resulting estimates. We compare our estimates for the Austin-Round Rock Metropolitan Area to published national-level estimates [27] of the proportion of each age group with underlying high risk conditions (Table A6). The biggest difference is observed in older adults, with Austin having a lower proportion at risk for complications for COVID-19 than the national average; for 25-39 year olds the high risk proportion is slightly higher than the national average.

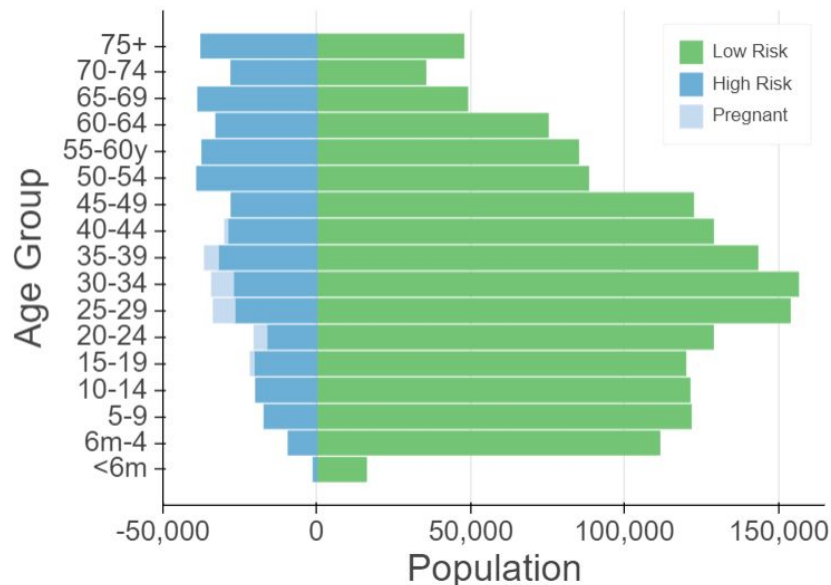


Figure A2. Demographic and risk composition of the Austin-Round Rock MSA. Bars indicate age-specific population sizes, separated by low risk, high risk, and pregnant. High risk is defined as individuals with cancer, chronic kidney disease, COPD, heart disease, stroke, asthma, diabetes, HIV/AIDS, and morbid obesity, as estimated from the CDC 500 Cities Project [17], reported HIV prevalence [20] and reported morbid obesity prevalence [21,22], corrected for multiple conditions. The population of pregnant women is derived using the CDC’s method combining fertility, abortion and fetal loss rates [28–30].

Table A4. High-risk conditions for influenza and data sources for prevalence estimation

Condition	Data source
Cancer (except skin), chronic kidney disease, COPD, coronary heart disease, stroke, asthma, diabetes	CDC 500 cities [17]
HIV/AIDS	CDC HIV Surveillance report [20]
Obesity	CDC 500 cities [17], Sturm and Hattori [21], Morgan et al. [22]
Pregnancy	National Vital Statistics Reports [28] and abortion data [29]

Table A5. Comparison between published national estimates and Austin-Round Rock MSA estimates of the percent of the population at high-risk of influenza/COVID-19 complications.

Age Group	National estimates [26]	Austin-Round Rock (excluding pregnancy)	Pregnant women (proportion of age group)
0 to 6 months	NA	8.1	-
6 months to 4 years	6.8	9.0	-
5 to 9 years	11.7	14.6	-
10 to 14 years	11.7	16.7	-
15 to 19 years	11.8	17.0	3.2
20 to 24 years	12.4	13.2	10.6
25 to 34 years	15.7	17.4	9.6
35 to 39 years	15.7	22.1	3.7
40 to 44 years	15.7	22.5	0.6
45 to 49 years	15.7	22.7	-
50 to 54 years	30.6	37.5	-
55 to 60 years	30.6	37.4	-
60 to 64 years	30.6	37.3	-
65 to 69 years	47.0	53.2	-
70 to 74 years	47.0	53.2	-
75 years and older	47.0	53.2	-

References

1. Seventh Amended Emergency Order for Public Health Emergency due to COVID-19. [cited

28 Apr 2020]. Available:

<https://co.jefferson.tx.us/documents/Coronavirus%20Docs/coronavirusdocs.htm>

1. Ionides EL, Nguyen D, Atchadé Y, Stoev S, King AA. Inference for dynamic and latent variable models via iterated, perturbed Bayes maps. *Proc Natl Acad Sci U S A*. 2015;112: 719–724.
2. Gao S, Rao J, Kang Y, Liang Y, Kruse J. Mapping county-level mobility pattern changes in the United States in response to COVID-19. *arXiv [physics.soc-ph]*. 2020. Available: <http://arxiv.org/abs/2004.04544>
3. Keeling MJ, Rohani P. *Modeling Infectious Diseases in Humans and Animals*. Princeton University Press; 2011.
4. Gillespie DT. Approximate accelerated stochastic simulation of chemically reacting systems. *J Chem Phys*. 2001;115: 1716–1733.
5. Liu Y, Gayle AA, Wilder-Smith A, Rocklöv J. The reproductive number of COVID-19 is higher compared to SARS coronavirus. *J Travel Med*. 2020;27. doi:10.1093/jtm/taaa021
6. R Core Team. *R: A Language and Environment for Statistical Computing*. Vienna, Austria: R Foundation for Statistical Computing; 2020. Available: <https://www.R-project.org/>
7. King AA, Nguyen D, Ionides EL. Statistical Inference for Partially Observed Markov Processes via the R Package pomp. *arXiv [stat.ME]*. 2015. Available: <http://arxiv.org/abs/1509.00503>
8. He X, Lau EHY, Wu P, Deng X, Wang J, Hao X, et al. Temporal dynamics in viral shedding and transmissibility of COVID-19. *Nat Med*. 2020. doi:10.1038/s41591-020-0869-5
9. Fox SJ, Pasco R, Tec M, Du Z, Lachmann M, Scott J, et al. The impact of asymptomatic COVID-19 infections on future pandemic waves. *medRxiv*. 2020. Available: <https://www.medrxiv.org/content/10.1101/2020.06.22.20137489v1.abstract>
10. Zhang J, Litvinova M, Wang W, Wang Y, Deng X, Chen X, et al. Evolving epidemiology and transmission dynamics of coronavirus disease 2019 outside Hubei province, China: a descriptive and modelling study. *Lancet Infect Dis*. 2020. doi:10.1016/S1473-3099(20)30230-9
11. He D, Zhao S, Lin Q, Zhuang Z, Cao P, Wang MH, et al. The relative transmissibility of asymptomatic COVID-19 infections among close contacts. *Int J Infect Dis*. 2020;94: 145–147.
12. Verity R, Okell LC, Dorigatti I, Winskill P, Whittaker C, Imai N, et al. Estimates of the severity of COVID-19 disease. *Epidemiology. medRxiv*; 2020. doi:10.1101/2020.03.09.20033357
13. CDC. People at High Risk of Flu. In: Centers for Disease Control and Prevention [Internet]. 1 Nov 2019 [cited 26 Mar 2020]. Available: <https://www.cdc.gov/flu/highrisk/index.htm>

14. CDC - BRFSS. 5 Nov 2019 [cited 26 Mar 2020]. Available: <https://www.cdc.gov/brfss/index.html>
15. Zhang X, Holt JB, Lu H, Wheaton AG, Ford ES, Greenlund KJ, et al. Multilevel regression and poststratification for small-area estimation of population health outcomes: a case study of chronic obstructive pulmonary disease prevalence using the behavioral risk factor surveillance system. *Am J Epidemiol*. 2014;179: 1025–1033.
16. Tindale L, Coombe M, Stockdale JE, Garlock E, Lau WYV, Saraswat M, et al. Transmission interval estimates suggest pre-symptomatic spread of COVID-19. *Epidemiology*. medRxiv; 2020. doi:10.1101/2020.03.03.20029983
17. 500 Cities Project: Local data for better health | Home page | CDC. 5 Dec 2019 [cited 19 Mar 2020]. Available: <https://www.cdc.gov/500cities/index.htm>
18. Health Outcomes | 500 Cities. 25 Apr 2019 [cited 28 Mar 2020]. Available: <https://www.cdc.gov/500cities/definitions/health-outcomes.htm>
19. Part One: Who Lives with Chronic Conditions. In: Pew Research Center: Internet, Science & Tech [Internet]. 26 Nov 2013 [cited 23 Nov 2019]. Available: <https://www.pewresearch.org/internet/2013/11/26/part-one-who-lives-with-chronic-conditions/>
20. for Disease Control C, Prevention, Others. HIV surveillance report. 2016; 28. URL: <http://www.cdc.gov/hiv/library/reports/hiv-surveillance.html> Published November. 2017.
21. Sturm R, Hattori A. Morbid obesity rates continue to rise rapidly in the United States. *Int J Obes*. 2013;37: 889–891.
22. Morgan OW, Bramley A, Fowlkes A, Freedman DS, Taylor TH, Gargiullo P, et al. Morbid obesity as a risk factor for hospitalization and death due to 2009 pandemic influenza A(H1N1) disease. *PLoS One*. 2010;5: e9694.
23. Estimating the Number of Pregnant Women in a Geographic Area from CDC Division of Reproductive Health. Available: <https://www.cdc.gov/reproductivehealth/emergency/pdfs/PregnancyEstimateBrochure508.pdf>
24. Miller GF, Coffield E, Leroy Z, Wallin R. Prevalence and Costs of Five Chronic Conditions in Children. *J Sch Nurs*. 2016;32: 357–364.
25. Cancer Facts & Figures 2014. [cited 30 Mar 2020]. Available: <https://www.cancer.org/research/cancer-facts-statistics/all-cancer-facts-figures/cancer-facts-figures-2014.html>
26. Hales CM, Fryar CD, Carroll MD, Freedman DS, Ogden CL. Trends in Obesity and Severe Obesity Prevalence in US Youth and Adults by Sex and Age, 2007–2008 to 2015–2016. *JAMA*. 2018;319: 1723–1725.
27. Zimmerman RK, Lauderdale DS, Tan SM, Wagener DK. Prevalence of high-risk indications for influenza vaccine varies by age, race, and income. *Vaccine*. 2010;28: 6470–6477.

28. Martin JA, Hamilton BE, Osterman MJK, Driscoll AK, Drake P. Births: Final Data for 2017. Natl Vital Stat Rep. 2018;67: 1–50.
29. Jatlaoui TC, Boutot ME, Mandel MG, Whiteman MK, Ti A, Petersen E, et al. Abortion Surveillance - United States, 2015. MMWR Surveill Summ. 2018;67: 1–45.
30. Ventura SJ, Curtin SC, Abma JC, Henshaw SK. Estimated pregnancy rates and rates of pregnancy outcomes for the United States, 1990-2008. Natl Vital Stat Rep. 2012;60: 1–21.